Near-contact interactions between a sphere and a plane

Cynthia E. Heath,* Shihai Feng, Joseph P. Day, and Alan L. Graham
Institute for Multiscale Materials Studies, Los Alamos National Laboratory, Los Alamos, New Mexico 87545, USA

Marc S. Ingber
Department of Mechanical Engineering, University of New Mexico, Albuquerque, New Mexico 87131, USA
(Received 15 September 2007; published 26 February 2008)

The hydrodynamic behavior observed for a sphere released under gravity in a Newtonian liquid is not consistent with that predicted by classical continuum theory when the sphere is near a solid wall. An irreversibility arises in the velocity of the sphere as it approaches and recedes from the plane that cannot be accounted for using continuum hydrodynamic equations alone. Earlier experiments on spheres falling from a plane were conducted under conditions such that this irreversibility could be attributed to the surface roughness of the spheres. In this investigation, we extend these studies to situations where the pressure field between the receding sphere and the plane drops to the vapor pressure of the fluid and cavitation occurs. Experimental data supports the theoretical prediction for a sphere's motion based on the irreversible effect of cavitation.

DOI: 10.1103/PhysRevE.77.026307 PACS number(s): 47.10.−g, 47.63.mf

I. INTRODUCTION

Understanding the governing phenomena of the motion between a sphere and a plane is essential for the advancement of our physical understanding of near-contact particle interactions. These interactions dominate the behavior of concentrated granular and suspension flows. Previous experiments have made significant progress toward correlating measured surface features of a non-colloidal particle to its near-contact behavior. Examples include the observations of spheres falling from mica sheets [1], passing in shear flows [2], rebounding from coated surfaces [3,4], and rolling down planes [5,6]. Still, the model for perpendicular motion between a sphere and plane is incomplete, as the irreversible nature of this motion has been studied only for a limited range of system parameters.

Classical continuum hydrodynamic theory provides a closed-form solution for a perfectly smooth sphere falling under a constant force toward a smooth plane in a Newtonian fluid at low Reynolds number. This solution predicts that the velocity of a sphere approaching a plane decreases in proportion to the decreasing separation distance but never reaches zero. It also predicts that the approaching and receding velocities are mirror images of each other and differ only in sign.

According to this solution, a sphere released from a certain position to settle for an arbitrary length of time toward a plane would never contact the surface, and upon reversal of the force on the sphere, it would take the same amount of time for the sphere to return to its original position. This reversible behavior is only observed experimentally if the sphere is not allowed to come too close to the plane. Once it comes to within a certain minimum separation distance, the sphere will take the same length of time to return to its starting distance no matter how long it was left to settle [1]. To predict the behavior of a sphere in motion near a plane, the source or sources of this irreversibility must be understood.

One source of irreversibility might be the breakdown of the continuum approximation in very small gaps. The fact that real fluids are not infinitely divisible is one obvious source of error in using the continuum assumption to analyze this problem. A sphere cannot be expected to continue approaching a plane when the gap between the two has reached the molecular dimensions of the fluid. The simulations of Challa and van Swol [7] showed that solvation forces become important when the gap is on the order of the fluid molecule size. This predominantly repulsive force would cause the approach velocity of a sphere falling under gravity to differ from its recession velocity. Other forces that would have irreversible effects on the velocity of a sphere are electroviscous [8] and van der Waals forces [9], which are significant only for very small, colloidal spheres.

For larger spheres, imperfections in the geometry of the system are another cause for the irreversible behavior observed. In this case, surface asperities determine the minimum separation distance between the sphere and the plane and, hence, the time required for the sphere to pull away under the force of gravity. Smart and Leighton [1] determined the effective hydrodynamic roughness of a sphere by measuring its fall time after allowing it to come to rest on a smooth surface and then inverting the system. They report that a sphere's effective hydrodynamic roughness, inferred from this fall time, is closely related to its physical roughness over the range of physical parameters examined in their investigation. A goal of the present work is to examine sphere-plane systems with a wider range of physical parameters.

The pressure drop generated behind a sphere as it falls away from a plane may be predicted by solving the fluid's equation of motion in bipolar coordinates [10], provided that the fluid is Newtonian and undergoes only creeping flow. The absolute pressure predicted in the region between the sphere and the boundary wall can be less than the fluid vapor pressure for spheres of more mass than those used in the experiments of Smart and Leighton [1]. Under these conditions, the fluid in the region of near-contact vaporizes, or cavitates. In a vaporized state, the fluid is unable to maintain

*heathc@lanl.gov

the tensile stress between the sphere and the plane that would exist in the liquid state, and the overall resistance on the falling sphere is greatly reduced. The sphere must fall to the distance where its pressure drop is no longer sufficient to sustain cavitation and the gap region again contains only liquid before its motion may be described by continuum hydrodynamics.

Evidence of cavitation in a different configuration has been shown by Prokunin [5] and Ashmore *et al.* [6], who both obtained photographs of a vapor bubble in the region between a rolling sphere and a plane where the absolute pressure is reduced to the vapor pressure of the liquid. Calculations of spheres rebounding from liquid-coated surfaces performed by Davis *et al.* [11] and Kantak and Davis [12] predict that the tensile force between a rebounding sphere and a plane is negligible while a vapor cavity is present. Barnocky and Davis [3] have also observed that the velocities of certain spheres are not affected by the fluid during rebound from a coated surface, due to cavitation in the film.

In this investigation, we focus on the fall times of sufficiently massive spheres, immersed in liquid, to confirm the presence and to quantify the effects of cavitation in certain near-contact sphere-plane systems. In the following section, the theoretical model for sphere-plane interaction is reviewed. Subsequent sections describe how irreversible phenomena may be incorporated into the theory and how our experimental data supports the cavitation prediction.

II. CLASSICAL CONTINUUM HYDRODYNAMIC THEORY

The exact solution to the Navier-Stokes equations for a smooth sphere falling slowly toward a plane in an otherwise unlimited fluid was obtained by Brenner [13] and Maude [14] in bipolar coordinates. The drag force on the sphere, expressed in the form of Stokes' law modified by a correction factor due to the proximity of the solid surface, is written as

$$F = 6\pi\mu a v \lambda, \tag{1}$$

where μ is the fluid viscosity, a is the sphere radius, v is the sphere velocity, and λ is the correction factor for a sphere falling perpendicular to a plane [15]. Stokes' law is valid only for "creeping flow" conditions, which require that inertial forces on the fluid are negligible and only viscous forces oppose the gravitational force on the sphere. The Reynolds number (Re) for flow around a sphere is equal to $av\rho_s/\mu$, where ρ_s is the sphere density. Creeping flow conditions may be assumed for $\mathrm{Re} < 0.1$ [16].

The exact value for λ may be obtained from the infinite series

$$\lambda(z) = \frac{4}{3}\sinh\alpha \sum_{n=1}^{\infty} \frac{n(n+1)}{(2n-1)(2n+3)} \times \left(\frac{2\sinh(2n+1)\alpha + (2n+1)\sinh(2\alpha)}{4\sinh^2\left(n+\frac{1}{2}\right)\alpha - (2n+1)^2\sinh^2(\alpha)} - 1 \right), \tag{2}$$

where $\alpha = \cosh^{-1}(1+h/a)$. The coordinate z is in the direction of the sphere's motion, and h is the minimum distance in this direction between the plane and the outside radius of the sphere as it falls. An approximation for λ is given by

$$\lambda(z) \approx 1 + \frac{a}{h}, \tag{3}$$

which approaches the exact value for both small and large gap widths [1].

For a sphere settling in a finite container, an additional correction factor must be incorporated to account for the lateral solid boundaries [17]. This will be called the parallel-wall correction factor k and will be expressed as

$$k = \frac{6\pi\mu a v \lambda}{F}. \tag{4}$$

Analytical solutions for k exist only for certain semi-infinite boundary geometries, such as an infinitely-long circular cylinder or two parallel plane walls [15]. For closed-ended cylinders of circular and square cross-section, numerical techniques have successfully been used to determine parallel-wall correction factors [18–20]. However, for a closed-ended rectangular tank, as is employed in our experiment, no analytical solution exists for k, and no previously-performed numerical analysis provides us with an approximation. Therefore, experimental techniques, as described in Sec. IV B, are used to obtain an individual correction factor k for each sphere, which accounts for the four lateral walls of our rectangular tank and the small inertial effects of the fluid on the particular sphere.

It will be assumed that the correction factors λ and k are independent of each other and that their superposition yields the overall velocity correction factor for the sphere falling in the closed container. The combination of Eq. (3) with our experimentally measured parallel-wall correction factor provides a more accurate value of the overall correction factor for our system than is obtained from either a boundary element simulation or a square-cylinder correction factor estimate [21].

Fall-time prediction

The Stokes' velocity describing the motion of a sphere falling in a fluid without boundaries is given by

$$v_{\mathrm{Stokes}} = \frac{2}{9}\frac{g\Delta\rho a^2}{\mu}, \tag{5}$$

where g is gravity, and $\Delta\rho$ is the difference in density between the sphere and the fluid. The velocity of a sphere falling from the surface of a tank may be calculated by performing a force balance for the quasi-static Stokes' approximation for the motion of a sphere near a plane. The velocity of the sphere as a function of z takes the form

$$v(z) = v_{\mathrm{Stokes}}\frac{k}{\lambda(z)}. \tag{6}$$

A sphere that falls with this velocity, where only viscous and pressure forces exert appreciable effects, will be said to fall "hydrodynamically." If its velocity is large enough, the

sphere will impact the plane elastohydrodynamically and undergo deformations that will affect the flow. The inertia of the sphere must dominate the viscous forces for elastic deformation to significantly affect its hydrodynamic behavior. Davis *et al.* [11] estimate that elastohydrodynamic effects become important for systems with Stokes numbers greater than 5, where the Stokes number is defined as

$$St = \frac{mv_0}{6\pi\mu a^2}.$$

Here, m is the mass of the sphere, and v_0 is the sphere's velocity as it contacts the surface. Stokes numbers for the spheres in this investigation were calculated to be on the order of 10^{-6} or smaller, so elastic deformations are neglected.

The predicted fall time for a sphere falling perpendicularly from a plane is the integral with respect to z of the inverse velocity from the starting distance h_1 to the final distance h_2. The starting distance h_1 is the point at which the sphere begins to fall hydrodynamically from the plane. Due to either the physical roughness or cavitation, h_1 will be nonzero, as explained in Sec. III, and the distance h_1 is not necessarily the sphere's smallest achievable distance from the plane. The only variable in Eq. (6) having z-dependence is λ, and by using Eq. (3), a simple integration of the inverse velocity may be performed to obtain

$$t_p = \frac{9\mu}{2g\Delta\rho a^2 k}\left[(h_2 - h_1) + a\left(\ln\frac{h_2}{h_1}\right)\right]. \tag{7}$$

This symbolic representation, made possible by the use of the approximation for λ, allows us to examine the functionality of the various physical parameters on the predicted fall time.

Because Eq. (3) always underestimates the exact value of λ, the predicted time calculated using Eq. (7) will always be less than that calculated by integrating Eq. (2) exactly. Predicted fall times were calculated using Eq. (7) for the range of spheres used in the experiment over the distance they would fall in the tank. These values were compared to fall times obtained using a finite-difference approximation to the integral of the series solution for λ. The maximum difference between the integral of the approximate λ and the approximate integral of the exact λ is 2.5%. This maximum error in the fall-time prediction occurs for the largest, most dense sphere used in the experiment, and it will be tolerated in order to retain the symbolic fall-time equation.

III. CONTINUUM HYDRODYNAMICS PLUS IRREVERSIBILITY

The model to be tested in this investigation combines the irreversible effects of near-contact interaction with the classical continuum hydrodynamic theory described in Sec. II. The aim is to determine the starting distance h_1 in Eq. (7), which results in an accurate fall-time prediction for spheres of varying size, density, and surface roughness receding from a near-contact condition. In this model, a fall time for a sphere approaching a plane may be predicted for arbitrary values of h_1 and h_2, up until the point where the sphere's surface roughness hinders its motion toward the solid boundary. At this point, the sphere is entering the near-contact region. Arbitrary h_1 and h_2 values may also be used to predict the receding fall time as long as the surface of the sphere remains outside the near-contact region and surrounded by liquid. An arbitrary starting distance h_1 may not be used if the sphere begins falling from within its near-contact distance.

The fall time of a noncavitating rough sphere, initially at rest on its surface features, may be predicted from Eq. (7) if its effective hydrodynamic surface roughness is used as the initial gap width h_1. Conversely, the definition of the effective hydrodynamic surface roughness δ_e is the initial gap width inferred from a fall-time measurement of a sphere, initially at rest, receding from a plane [1]. A false δ_e value will be obtained, however, if the sphere is small enough to be affected by colloidal forces or massive enough to cause the fluid to cavitate behind it as it falls. To determine if cavitation will occur, the pressure drop in the region between the plane and the sphere must be calculated using classical hydrodynamic theory.

A. Pressure drop

The first-order term in the Taylor series expansion of the solution for the change in fluid pressure at the point of closest approach between a sphere and a plane is given by [22]

$$\Delta p = \frac{\left(1 - \frac{h}{a}\right)3\mu v a}{h^2}. \tag{8}$$

Reversible behavior is observed in this model, so the pressure drop for a receding sphere will be equal in magnitude but opposite in sign to that for an approaching sphere. This solution is valid for small gap widths only ($h/a \ll 1$), and for very small gap widths, the h/a term is insignificant. The nondimensional gap widths over which cavitation is expected for the spheres in the current experiment are $O(10^{-3})$, so the h/a term will be ignored [21]. Substituting Eq. (6) for v, and using Eq. (3) for λ, the Δp value may be approximated for small gaps as

$$\Delta p \approx \frac{2}{3}\frac{g\Delta\rho a^3 k}{(h^2 + ah)}. \tag{9}$$

Equation (9) will be used to estimate the pressure drop behind a sphere that begins with its physical roughness features in contact with a plane and then, after the direction of the force acting on the sphere is reversed, separates from the plane. By subtracting Δp from the tank fluid pressure, the total pressure in the gap is calculated, which determines the phase of the fluid. Hydrostatic pressure gradients are ignored in this pressure calculation. As long as the total pressure is less than the vapor pressure of the liquid, the upward force acting on the sphere will be greatly reduced from that in the noncavitating case [11,12]. In particular, the sphere will fall quickly to the point at which the pressure in the gap is greater than the vapor pressure, where it will begin to fall according to Eq. (6).

The quadratic formula may be used to calculate the cavitation distance $h_{\Delta p}$, which is defined by the value of h for which the pressure drop is equal to the difference between the atmospheric pressure p_{atm} and the vapor pressure p_{vap} of the liquid. That is, the cavitation distance is the distance from the plane where cavitation ceases and the sphere begins to fall hydrodynamically, and it is found to be

$$h_{\Delta p} = \frac{a}{2}\left(-1 + \sqrt{1 + \frac{8}{3}\frac{g\Delta\rho a k}{(p_{\text{atm}} - p_{\text{vap}})}}\right). \tag{10}$$

Only the positive square root is considered, because the distance $h_{\Delta p}$ must be positive.

If the sphere's physical roughness asperities prevent it from coming as close as $h_{\Delta p}$ from the plane, the liquid will not cavitate during separation, and the sphere will fall hydrodynamically from an initial gap width equal to its effective hydrodynamic roughness. Smart and Leighton [1] obtained effective hydrodynamic surface roughness values that were between the average roughness and the maximum peak-to-valley roughness values measured directly on their sphere surfaces. If the effective hydrodynamic roughness is smaller than $h_{\Delta p}$, in our model, the initial distance from which the sphere falls hydrodynamically is $h_{\Delta p}$. Retaining the h/a term in Eq. (8) results in a difference in cavitation distance of less than 0.5% for the spheres used in the present experiment. The corresponding fall-time difference is less than 2 ms, which is much smaller than the uncertainty in the timing of our experiments, to be discussed in Sec. IV.

From the pressure drop solution provided by Brenner [10], the fluid state may be determined at any radial distance from the point of closest approach at the center, provided it remains within the small gap region (where $h/a \ll 1$). Using this solution, the radius of the area of cavitation may be calculated as the sphere's distance from the plane increases. The cavitation area increases from zero radius, as the sphere begins its separation, to its maximum radius. At this point, the region of vaporized fluid is a thin disk of very little volume. For the spheres that are predicted to cause cavitation in the current experiment, the ratios of maximum cavity diameter to cavity thickness were calculated to be greater than 70. From its maximum size, the cavity's radius is predicted to shrink smoothly back to zero. The time scale for the evolution of the vapor cavity is unknown, so the acoustic effects of the collapse are uncertain. Because the cavity is highly aspherical, the role of acoustic emission in the damping of the bubble collapse is expected to be small [23]. In our model, when the vapor bubble has disappeared the sphere is expected to immediately begin its hydrodynamic descent, unaffected by the bubble collapse.

B. Cavitation prediction

In order to compare spheres of different density, radius, and roughness, a nondimensional parameter called the cavitation number will be used. The cavitation number C is defined as the pressure drop required to vaporize the liquid normalized by Δp_0, the dynamic pressure drop generated by the moving object [24], and it takes the form

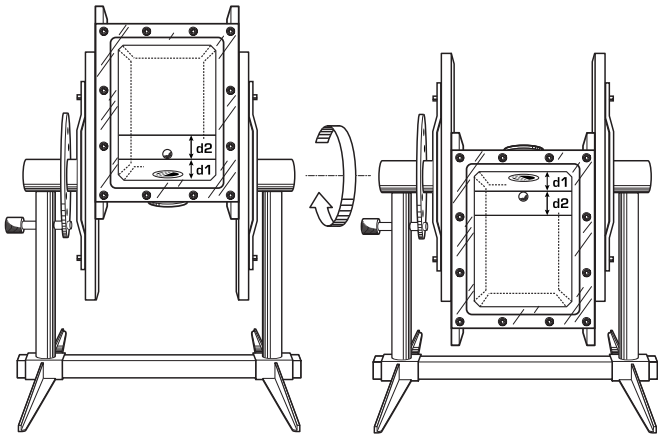

FIG. 1. Experimental tank in upright and inverted positions. Fall-time measurements were made as the sphere traveled distances d_1 and d_2 on both approach and recession from the mica disk affixed to the tank bottom. The fall time obtained for d_2 characterizes the experimental system, and the time for d_1 provides information about the near-contact interaction between the sphere and the plane.

$$C = \frac{p_{\text{atm}} - p_{\text{vap}}}{\Delta p_0}. \tag{11}$$

The dynamic pressure drop for a near-contact sphere will be defined as the maximum pressure drop that would be generated by the sphere as it fell from a plane if no cavitation occurred. This value is calculated from Eq. (9), using the sphere's effective hydrodynamic surface roughness δ_e as the minimum separation distance, and it is given by

$$\Delta p_0 = \frac{2}{3}\frac{g\Delta\rho a^3 k}{(\delta_e^2 + a\delta_e)}. \tag{12}$$

A sphere of cavitation number less than 1 will develop a dynamic pressure drop larger than that required to vaporize the liquid. Different measures of physical surface roughness may be obtained by surface profilometry, but, as will be discussed later, it is difficult to select the physical roughness value that matches the sphere's effective hydrodynamic roughness value.

IV. EXPERIMENT

Experimental tests were performed in a rotatable liquid-filled tank of inner dimensions $17.145 \times 12.065 \times 12.065$ cm^3, as shown in Fig. 1. A freshly cleaved mica disk was attached to the bottom of the tank to provide a molecularly smooth surface. Hence, most of the roughness effects on a sphere's motion may be attributed to its own surface features. The rotation mechanism was designed so that the axis of rotation was aligned with the bottom surface of the tank. This feature ensured that moments induced on the sphere by the fluid during rotation were minimized in the region of the sphere-plane contact point.

While the tank was in its upright position, a sphere was allowed to settle toward the mica sheet for a time longer than that for which the motion was known to be reversible. To reverse the motion of the sphere, the tank was inverted over

TABLE I. Sphere statistics.

Material	Grade	a (mm)	ρ_s (kg/m^3)	δ_a (nm)	δ_q (nm)	δ_p (nm)
WC[a]	25	6.340 ± 0.0025	14791 ± 17	17 ± 1	20 ± 2	105 ± 11
WC[a]	25	3.172 ± 0.0017	14996 ± 24	24 ± 6	30 ± 7	195 ± 35
WC[a]	25	2.380 ± 0.0025	15022 ± 47	22 ± 6	26 ± 7	105 ± 25
CS[a]		3.171 ± 0.0028	7806 ± 10	35 ± 11	49 ± 22	355 ± 317
WC[a]	25	2.775 ± 0.0025	14909 ± 40	67 ± 26	90 ± 32	788 ± 186
WC[a]	25	1.988 ± 0.0025	14924 ± 56	41 ± 6	53 ± 7	442 ± 106
WC[b]	25	1.186 ± 0.0025	15161 ± 96	17 ± 5	21 ± 6	112 ± 25
WC[a]	25	1.587 ± 0.0009	14942 ± 25	32 ± 11	41 ± 19	221 ± 170
WC[b]	25	0.795 ± 0.0013	14789 ± 73	27 ± 8	31 ± 9	137 ± 40
AO[a]		3.171 ± 0.0022	3848 ± 8	68 ± 25	148 ± 81	2507 ± 1189
Br[b]	200	2.002 ± 0.0025	8759 ± 33	255 ± 99	321 ± 124	2325 ± 258
WC[b]	25	0.598 ± 0.0025	14214 ± 179	43 ± 8	56 ± 11	422 ± 90
WC[b]	25	0.398 ± 0.0009	14758 ± 107	22 ± 7	27 ± 9	133 ± 45
Br[b]	200	1.586 ± 0.0015	8523 ± 24	316 ± 63	455 ± 107	4515 ± 597
Br[b]	200	1.193 ± 0.0008	8519 ± 17	196 ± 34	261 ± 37	2878 ± 418
Br[b]	200	0.798 ± 0.0016	8342 ± 50	355 ± 145	466 ± 186	3275 ± 625
Br[b]	200	0.598 ± 0.0018	8444 ± 77	245 ± 22	313 ± 18	2360 ± 642
Br[b]	200	0.405 ± 0.0016	8384 ± 106	295 ± 99	364 ± 108	2198 ± 478
Br[b]	200	0.260 ± 0.0026	8178 ± 281	349 ± 158	459 ± 223	3110 ± 1261

[a]Fluid used in experiment: UCON 75-H-90000.
[b]Fluid used in experiment: UCON 75-H-9500.

a period of less than 1 s. At the midpoint of the rotation of the tank, the stopwatch was started, and the time was marked as the sphere passed the lines on the tank demarcating distances d_1 (3.19 cm from the mica) and d_2 (5.70 cm from d_1). Lines at equal distances on both the front and back of the tank were visually aligned during each time measurement. The experimental measurement of interest is the time elapsed between when the tank was inverted and when the sphere had traveled distance d_1.

The fall time over distance d_2 was measured as the sphere fell toward the mica sheet and again as it fell away. The average fall time over d_2 for all repetitions of an experiment was used to determine the parallel-wall correction factor for each sphere, as will be explained in Sec. IV B. The number of repetitions performed for an experiment depended on the total time required for the sphere to fall. As few as 6 and as many as 49 trials were performed for particular spheres. This resulted in a fall-time uncertainty of less than 1.2%, based on a level of confidence of 95% for each experiment [21].

A. Physical measurements

Polyalkalene glycol liquids of two different viscosities were used as the experimental fluids, UCON 75-H-90000 and UCON 75-H-9500 (Dow Chemical Co., Midland, MI). The liquid viscosity for each experiment was chosen to ensure that the fall time for each sphere was long enough to measure accurately yet short enough to repeat a statistically significant number of times in a single laboratory session. The less viscous 75-H-9500 liquid was used for all brass spheres and for the tungsten carbide spheres smaller than 1.2 mm in radius. All other experiments were performed using the 75-H-90000 liquid.

The liquid viscosity is strongly dependent on temperature, so thermally stable laboratory conditions were essential to minimize viscosity gradients inside the tank. The ambient laboratory temperature was measured to be 21.72 ± 0.36 °C during the period that the experiments were performed. Fluid densities and viscosities were measured for both types of liquid at temperatures between 19 and 26 °C, a range much larger than that observed in the laboratory. Temperature-viscosity functions were developed from Ubbelohde viscometer tube measurements and used to determine the fluids' viscosity ranges for the small range of thermal conditions in the laboratory [21]. The resulting viscosities were 46.76 ± 0.55 Pa s and 5.05 ± 0.16 Pa s for the 75-H-90000 and 75-H-9500 liquids, respectively. A temperature-density relationship was also established from pycnometer measurements and yielded a density of 1091.86 ± 0.39 kg/m^3 for both types of liquid over the laboratory's temperature range [21].

A range of sizes of tungsten carbide (WC) and brass (Br) spheres were used in the experiments to test the functionality of the cavitation model. Single spheres of hardened chrome steel (CS) and aluminum oxide (AO) were also used to compare the hydrodynamic behavior of different materials. Sphere radii ranged from 6.34 to 0.153 mm, and statistics for each sphere are presented in Table I, in order of increasing cavitation number. Because spheres of the same material were found to have somewhat different density and roughness values, the order of increasing cavitation number is not necessarily the order of decreasing radius for a sphere series.

For example, the WC sphere of radius 1.186 mm has a smaller cavitation number than the 1.587 mm sphere, due to its larger density and smaller roughness. Radius values were obtained from multiple diameter measurements for the larger spheres, using a Starrett digital caliper. The smaller spheres were measured using a Nikon MM-60 measuring microscope (Nikon Corp., Yokohama, Japan) and the diameter calculation function of a Quadra-Chek 200 geometric readout (Metronics, Inc., Bedford, NH). Material densities were calculated from radius and mass measurements and are listed for each sphere in Table I. The mean values for the WC, Br, CS, and AO spheres were 14857, 8588, 7806, and 3848 kg/m^3, respectively.

The series of WC spheres was chosen to demonstrate the presence of cavitation. These were predicted to be massive enough to generate the pressure drop required for cavitation while still falling slow enough to assure the creeping flow condition required by Eq. (1). The Reynolds number associated with the terminal velocity of the most rapidly falling sphere was calculated to be 0.017, and the fluid shear rate at the equator of the falling sphere was calculated to be less than 11 s^{-1} for all experiments. Previous measurements have shown UCON liquids to be Newtonian up to shear rates of 10^3 s^{-1} [25].

To examine the irreversible behavior of both cavitating and noncavitating systems using commercially available balls, it was necessary to perform experiments with spheres of different materials. Since the lower size limit of commercially available WC balls had already been reached, Br balls were selected for the noncavitating experiments. Much smaller diameters were available in this material, although the surfaces were not to be nearly as smooth as the WCs, due to the ductility of the Br. Commercially produced balls must conform to the standards of ANSI/AFBMA Std. 10-1983, which prescribes specific dimensional tolerance requirements for each ball grade. All WC spheres were ordered to be grade 25, which has a basic diameter tolerance of ± 0.0025 mm, a maximum deviation from spherical form of 0.0006 mm, and an upper limit for average surface roughness of 51 nm. Average roughness δ_a is defined as the average of every surface height data point Z_i acquired over the sample area, where Z_i is the distance from the measured point to the mean plane. It is written as

$$\delta_a = \frac{1}{N}\sum_{i=1}^{N} |Z_i|,$$

where N is the number of data points. Brass spheres were obtained in the best grade available, grade 200, which has a basic diameter tolerance of ± 0.025 mm, an allowed spherical deviation of 0.005 mm, and a maximum δ_a of 203 nm. Because the effective hydrodynamic roughness is closely related to the physical surface roughness for noncavitating spheres, the cavitation numbers for the grade 200 Br spheres are larger than they would have been for grade 25 Br spheres.

A variety of measures is available to quantify physical surface roughness, but no directly-measured quantity has been shown to equal the effective hydrodynamic roughness of a sphere. The appropriate measure of the physical roughness to use in calculating the dynamic pressure drop from Eq. (12) is, therefore, uncertain. Of the spheres investigated in the experiment, none had a smooth surface with protrusions of a uniform height that could be used as an obvious physical roughness value. Rather, the manufacturing processes used to polish the spheres leave the surfaces covered with nonuniform asperities, scratches, and pits, resulting in profiles that cannot be easily quantified by a single number. Surface height profiles were obtained by interferometry for each sphere using a Wyko NT2000 Optical Profiler (Veeco Metrology Group, Tucson, AZ), and statistical values including average, peak, and root-mean-square (rms) roughness were calculated. Peak roughness δ_p is the height difference between the highest point and the lowest point measured in a sample area, and rms roughness δ_q is defined as

$$\delta_q = \sqrt{\frac{1}{N}\sum_{i=1}^{N} Z_i^2}.$$

The Vision32 software used to analyze the acquired data uses the digital approximations for the three-dimensional average and rms roughnesses given by

$$\delta_a = \frac{1}{MN}\sum_{j=1}^{M}\sum_{i=1}^{N} |Z_{ji}|$$

and

$$\delta_q = \sqrt{\frac{1}{MN}\sum_{j=1}^{M}\sum_{i=1}^{N} Z^2(x_i, y_j)}, \tag{13}$$

where M and N are the number of sampled data points in the x and y direction, respectively [26]. The average and peak roughnesses may be referred to as the "minimum" and "maximum" roughness values for a sample area. The rms roughness, as calculated by Eq. (13), is equivalent to the standard deviation of the surface height data, and it will be the preferred value for characterizing a sphere surface in our study. rms roughness is more sensitive to large surface features than average roughness and more repeatable than peak roughness.

The sample area over which these roughness values were calculated was determined by the ball size and an initial supposition of the roughness value. We define the supposed roughness δ_s to be the maximum allowable δ_a for the sphere grade. Using the estimate for the interaction area of $2\pi\delta_s a$ provided by Smart and Leighton [1], area sizes appropriate for each sphere were calculated. Average, rms, and peak roughnesses were evaluated over these areas for each sample obtained on each sphere.

Two sets of six samples taken at random locations on the same sphere were obtained for the brass spheres of radii 0.260 and 1.586 mm. For both spheres, mean values of δ_a, δ_q, and δ_p for the first set of six samples agreed with the mean values for the second set of six samples to within the 95% confidence limits determined for the sample sets. Having established the sample size of six as being statistically adequate, surface profile samples were acquired at six ran-

domly selected locations around the surface of each sphere. The mean values of δ_a, δ_q, and δ_p are listed for each sphere in Table I, with uncertainties equal to the standard deviation of the six samples. It may be noticed that one WC sphere and all but one Br sphere had values of δ_a that were larger than the limit set by their grade. The mean of all δ_q values obtained for the WC spheres was 39 nm, and the mean for the Br spheres was 377 nm.

The question may arise as to whether the surface roughness should be added to or subtracted from the sphere's radius for the purpose of calculating the predicted fall time. Upon investigating Eq. (7), it may be found that t_p is much more sensitive to incremental changes in the parameter h_1 than to changes in a. This indicates that the importance of the surface roughness lies in its effect on the initial gap width and not the sphere's radius. The measured radius uncertainties were approximately 2 μm, which is more than 4 times greater than any of the spheres' δ_q values. Therefore, the spheres' measured radius values will not be modified to include the surface roughness for calculation of the predicted fall times.

The surfaces of the WC series and the Br series were qualitatively similar, having been polished with the same grinding and lapping technique. Height profiles for these spheres were mostly random, with the Br surfaces exhibiting more deep pits than the WC. The CS sphere had very few pits but many long scratches, and the surface of the AO sphere was dominated by pits.

The effective hydrodynamic roughness δ_e for a particular sphere is expected to be bounded by the minimum and maximum physical roughness [1,9,27], but these measurements can differ by as much as two orders of magnitude. The actual δ_e value may only be obtained by performing a fall-time measurement on a noncavitating system. Smart and Leighton noted that the δ_e values inferred from their fall-time measurements were greater than their average roughness values and close to one-half of their peak roughness values [1]. In the following section, fall times for noncavitating systems will be used to relate our rms roughness measurements to effective hydrodynamic roughness values for our spheres.

A new mica disk was cleaved, characterized, and attached to the tank bottom each time the liquid in the tank was changed. Grade V-4 muscovite mica (Structure Probe, Inc., West Chester, PA) was used, which provided a smooth layer of molecules for the near-contact interaction with the rough sphere. Three different mica disks were used in the experiments, and roughness measurements were obtained for six sample areas on each disk, using a Wyko RST Plus Optical Profiler (Wyko Corp., Tucson, AZ). rms roughness values were evaluated over sample areas of 50 μm diameter, a size comparable to the interaction areas for the largest spheres. The mean of all δ_q values measured for the mica disks was 0.7 nm. Being more than an order of magnitude smaller than the roughness values of the spheres, the mica roughness will be neglected in the determination of the initial gap between the sphere and the plane.

Other parameters required to calculate cavitation numbers and distances are gravity and the pressure drop necessary for fluid vaporization. The local value for gravity used in our calculations was estimated by the National Geodetic Survey of the National Oceanic and Atmospheric Administration in 1977. Elevation and a Bouguer anomaly are accounted for in the value of $9.791\ 11 \pm 0.000\ 04\ \mathrm{m/s^2}$. The average value for the local atmospheric pressure over the course of the experiments was 787 kPa with deviations of up to 23 kPa due to changing weather conditions. The vapor pressure reported on the MSDS for both varieties of UCON oil was 1.3 Pa. In calculating the cavitation distance from Eq. (10), we assume equilibrium behavior with no delay in the liquid vaporization or bubble collapse.

B. Parallel-wall correction factor measurement

The parallel-wall correction factor for a sphere is determined from a measurement of the time that it takes to fall distance d_2 in the experimental tank. The effect of the vertical tank walls may be measured by comparing the velocity of the sphere in this section with its Stokes' velocity. In this region of the tank, the velocity of the sphere is independent of the surface roughness [28]. Also, the end effects of the top and bottom tank surfaces will be considered negligible, because the bottom surface is removed by at least five particle radii for all spheres [20,29]. Therefore, the perpendicular-wall correction factor λ will be considered one, and we will use the ratio of the measured velocity to v_{Stokes} to calculate the correction factor due to the four lateral walls. By using the expression

$$k = \frac{v}{v_{\mathrm{Stokes}}} \tag{14}$$

in Eq. (7), the physical parameters g, $\Delta\rho$, a, and μ are eliminated from the fall-time prediction for noncavitating spheres. Smart and Leighton similarly remove the importance of these quantities by normalizing their experimental fall time with the fall time of the same sphere through a distance farther away from the plane [1]. The values of g, $\Delta\rho$, a, and μ are still required to calculate a cavitation distance, so for spheres of $C<1$, the fall-time prediction is not independent of these parameters.

C. Experimental results

Measured fall times are compared to predicted fall times to determine the validity of the cavitation hypothesis. The expression given by Eq. (7) is used to predict the time a sphere will take to fall through the liquid from an initial distance from the plane, h_1, to a final distance, in this case, d_1. These fall-time predictions were calculated for each sphere using three different initial distances, the sphere's rms roughness, the sphere's peak roughness, and the sphere's cavitation distance. In Fig. 2, these three fall-time predictions are indicated for each sphere by a triangle, a diamond, and a circle, respectively. A profile of the sphere's fall time is included as either a solid or dashed line, which represents the sphere's total fall time starting from an arbitrary initial distance from the plane. The solid line profiles and open symbols are used for the six WC balls dropped in the 75-H-90000 liquid. The cavitation numbers for these spheres are all less than 1, whether the minimum or maximum roughness

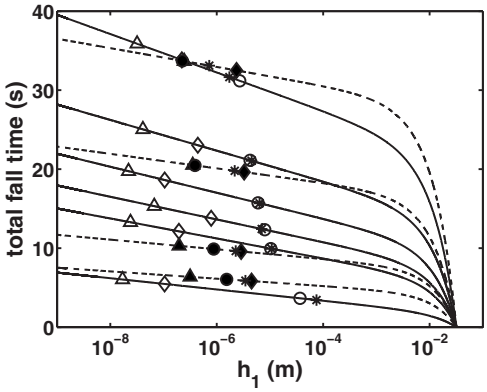

FIG. 2. Total fall time vs initial distance from the plane for six WC spheres and four brass spheres. Predictions for WC spheres are displayed as open symbols and solid lines, and predictions for brass spheres are displayed as solid symbols and dashed lines. From the measured fall time, indicated by an asterisk, the initial distance of a sphere from the plane is inferred. The initial distance implied by each WC experiment is greater than both the rms roughness and peak roughness for a particular sphere and is in agreement with the predicted cavitation distance. Initial distances implied by the brass experiments are similar to the peak roughness values measured for the spheres.

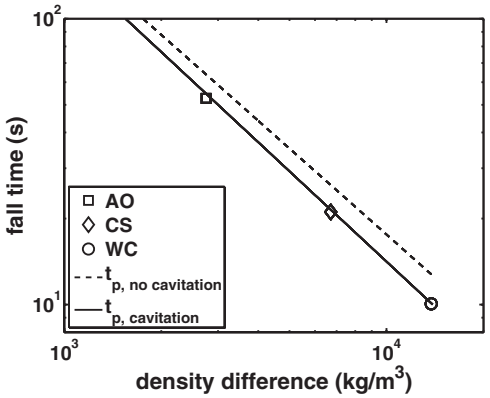

FIG. 3. Fall time vs density difference for 3.17 mm radius spheres. Experimental measurements for spheres of aluminum oxide, chrome steel, and tungsten carbide agree with the functionality of the cavitation model.

is used to calculate C. The dashed line profiles and solid symbols are used for four Br balls dropped in the 75-H-9500 liquid. The cavitation numbers for these spheres are all greater than 1 if the peak roughness is used to calculate C. The experimentally-measured fall time for each sphere is indicated by an asterisk.

The initial gaps implied by the experimental measurements for the WC spheres of $C<1$ are consistent with the hypothesis that the spheres are falling hydrodynamically from their cavitation distances rather than their physical roughness heights. The error bars indicating the 95% confidence limits of the measured times are smaller than the symbols used to represent the data points. The initial gaps implied by the experiments using the Br spheres of $C>1$ are very close to the measured physical roughness values of the spheres.

In the classical hydrodynamic model, the time predicted for a sphere to fall from a plane is inversely related to the density difference between the sphere and the liquid, as can be seen from Eq. (7). For a sphere of radius 3.17 mm falling through a liquid of viscosity 46.76 Pa s from an initial gap of 80 nm, the predicted fall time as a function of density difference is calculated to be

$$t_{p,\text{no cavitation}} = 175\ 827(\Delta\rho)^{-1} \tag{15}$$

if no cavitation occurs. However, this relationship is lost when the sphere's initial gap is equal to its cavitation distance, which is a function of the density difference. By substituting $h_{\Delta p}$ into the symbolic approximation to the fall time given by Eq. (7), the more complicated dependence of t_p on $\Delta\rho$ may be seen. Assuming cavitation does occur in the system described above, the inverse relationship of Eq. (15) becomes a power-law function of $\Delta\rho$ given by

$$t_{p,\text{cavitation}} = 222\ 476(\Delta\rho)^{-1.0492}. \tag{16}$$

The parallel-wall correction factor used to generate Eqs. (15) and (16) was taken to be 0.885, the average of the measured k values for the three spheres of radius 3.17 mm used in the experiment. The k values measured for the AO, CS, and WC spheres were 0.882, 0.886, and 0.887, respectively. The mean δ_q value for these three spheres, 80 nm, was used as the initial gap width in the calculation of Eq. (15).

Figure 3 shows the measured fall times for the three spheres of radius 3.17 mm studied in the 75-H-90000 liquid, which were all expected to cavitate during separation. The functions of Eqs. (15) and (16) are shown for comparison, and the data points agree well with Eq. (16), which includes cavitation in the hydrodynamic model. The 95% confidence limits are contained within the dimension of the data point symbols.

To compare experiments spanning four orders of magnitude of cavitation number performed with different materials and fluid viscosities, a unitless representation of the data is helpful. The data is nondimensionalized by dividing the experimental time by t_{Stokes}, the time the sphere would take to fall through a certain distance at its Stokes' velocity. This velocity will be integrated over the distance d_1, yielding

$$t_{\text{Stokes}} = \frac{9\mu(d_1)}{2g\Delta\rho a^2}. \tag{17}$$

The chosen distance d_1, while arbitrary, represents a characteristic length scale for the present experiment.

The nondimensional parameter S will be defined as

$$S = \frac{t_{\delta_e} - t_{\text{meas}}}{t_{\text{Stokes}}}, \tag{18}$$

where t_{δ_e} is the time predicted using Eq. (7) for a sphere to fall from its effective hydrodynamic roughness to d_1, and t_{meas} is the time recorded for the sphere to fall to d_1 in the experimental tank. A large value of S indicates a measured time that is much smaller than the fall time predicted assuming the sphere fell hydrodynamically from its δ_e value. The

δ_e for a noncavitating system is the roughness value used to minimize S, as explained below. The four smallest Br spheres have cavitation numbers greater than 1 regardless of whether their minimum or maximum roughness is used, so they may be considered noncavitating systems. A relationship between measured rms roughness and effective hydrodynamic roughness will be determined from the fall-time measurements of these four spheres by minimizing a generalized error function.

The generalized error between the measured and predicted values for these experiments is defined as the sum of the absolute values of S for the four smallest Br spheres, written as

$$E = \sum_{n=1}^{4} |S_{\mathrm{Br}_n}|.$$

The generalized error E was calculated using a range of normalized roughness values for t_{δ_e} [21]. The roughness was normalized by 377 nm, the mean of the δ_q values measured for all seven Br spheres. The minimum E value, 0.076, corresponded to a normalized roughness of 1.5, implying that the measured rms roughness provides a slightly low estimate of the effective hydrodynamic roughness for these Br spheres. The δ_q value for each Br sphere will, therefore, be increased by a factor of 1.5 to obtain the δ_e value for use in the data analysis. Noting the qualitative similarity between the Br and WC surfaces, the same factor will be applied to the δ_q values of the WC series. With these effective hydrodynamic roughness values, we may now calculate specific cavitation numbers for all spheres and predict fall times for spheres with $C>1$. As mentioned in Sec. IV A, the unmodified radius measurement is used to calculate the predicted fall time for a sphere. The effective hydrodynamic roughness will simply be imposed on the outer surface to set the lower limit on the gap between the sphere and the plane.

A predicted value for S may be calculated using Eq. (7) to predict t_{meas} using the cavitation distance as the initial gap for spheres of $C<1$. After reduction,

$$S_{\mathrm{pred}} = \frac{1}{k(d_1)}\left[h_{\Delta p} - \delta_e + a\left(\ln\frac{h_{\Delta p}}{\delta_e}\right)\right]. \tag{19}$$

Because $h_{\Delta p}$ may be replaced with δ_e for noncavitating spheres, S_{pred} is zero for all spheres of $C>1$, regardless of material. In Fig. 4, the S_{pred} values for all spheres are shown as circles. These predictions are obtained using the values of $\Delta\rho$, k, and δ_e calculated individually for each sphere. A cavitation-dominated irreversibility for the near-contact interaction is predicted by a nonzero S_{pred} value, and a roughness-dominated irreversibility is predicted by a zero value. The experimental measurements for the WC and Br spheres are shown by triangles and inverted triangles, respectively.

The error bars for each data point were obtained by propagating the uncertainty in each physical measurement to the uncertainty in S. For an expanded version of Eq. (18), given by

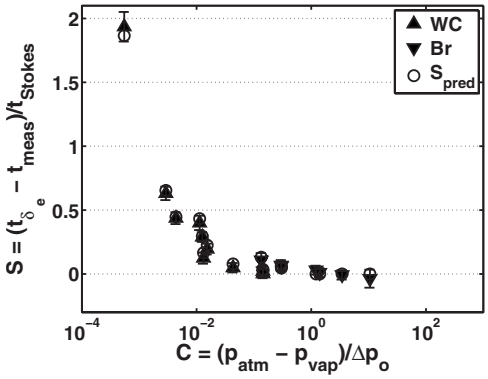

FIG. 4. Cavitation number vs S. An effective hydrodynamic roughness value equal to 1.5 times the sphere's rms roughness was used for both the tungsten carbide and brass sphere series. Experimental data is consistent with the cavitation model for $C<1$ and the physical roughness model for $C>1$.

$$S = \frac{1}{kd_1}\left[h_2 - \delta_e + a\left(\ln\frac{h_2}{\delta_e}\right)\right] - \frac{t_{\mathrm{meas}}}{d_1}\frac{2g\Delta\rho a^2}{9\mu}, \tag{20}$$

error propagation formulas were used to determine the uncertainty due to each parameter and, finally, the overall uncertainty in S for each data point [21]. The uncertainty associated with the parallel-wall correction factor is the dominant source of the overall uncertainty, contributing 30–80% for each sphere. The roughness measurement uncertainty is the next most significant, accounting for as much as 54% of the overall error bar length.

Each experimental data point agrees with its corresponding prediction to within the uncertainty of the measurement, and the divergence of t_{meas} from t_{δ_e} is apparent for small cavitation numbers. Both the WC and brass spheres below $C=1$ match the cavitation predictions, and the Br spheres above $C=1$ match the roughness predictions. Fall times for all cavitating spheres, which are independent of their estimated δ_e values, were predicted to within 3%. The initial gap for these cavitating spheres could be predicted based on knowledge of just the atmospheric and vapor pressures, besides the values of g, $\Delta\rho$, a, and k, which are required for the basic hydrodynamic fall-time predictions. Although the values of δ_e are not necessary to calculate fall times for cavitating spheres, they are required to calculate C values, which provide a measure of the likelihood that cavitation will occur, a useful parameter in the comparison of data points for a variety of sphere-plane systems. Fall times for the noncavitating spheres, which are highly dependent on the estimated δ_e values, were predicted to within 4%.

The transition from one irreversible behavior to another at $C=1$ is evident. Fall times for the WC spheres and the larger Br spheres agree with the cavitation prediction, and those for the smaller Br spheres agree with the roughness prediction. The fact that the data points for the Br spheres match the predictions to within the measurements' uncertainties confirms that $1.5\delta_q$ is an appropriate value to use for δ_e. While the effective hydrodynamic roughness does not affect the fall time for cases in which $C<1$, it is the dominant source of irreversibility for cases in which $C>1$.

V. CONCLUSIONS

By conducting simple, well-characterized macroscale experiments, data is obtained revealing microscale information about near-contact interactions. The experimental data confirms that classical continuum hydrodynamic theory may be used to model the motion of a sphere falling from a plane if the correct initial gap distance is known. If the cavitation number for the system is greater than 1, this initial gap is equal to the effective hydrodynamic surface roughness. If the cavitation number is less than 1, the cavitation distance should be used as the initial gap. This is the distance over which the fluid behind the sphere is in a vapor state and cannot sustain the stress predicted by the hydrodynamic equations.

The cavitation number is highly dependent on the physical roughness of the sphere surface, and for a system with a cavitation number very close to 1, the dominant source of irreversibility is difficult to determine. Effective hydrodynamic roughness values were found to exceed physical rms roughness values by a factor of 1.5. This is consistent with the finding of Smart and Leighton [1] that the measured effective hydrodynamic roughness is of the same order as the physical surface roughness. However, this particular relationship may not hold for all sphere grades or materials. Inferring an initial gap from a sphere's measured fall time remains the only reliable method of determining an effective hydrodynamic surface roughness and, hence, an accurate cavitation number. With knowledge of the system's cavitation number, the irreversibility exhibited in a macroscale sphere-plane interaction at low Reynolds number may be attributed to either physical roughness or cavitation.

ACKNOWLEDGMENTS

The authors would like to thank Professor Howard Brenner for the guidance on selecting the most appropriate form of his solution for the pressure drop between a sphere and a plane. Gratitude is also extended to Dr. Robert Day for the hours of patient instruction on the various tools used for sphere measurement and characterization. The authors sincerely thank Dr. Joanne Wendelberger for her assistance in performing the error propagation calculations. The authors also appreciate Professor Jacob Israelachvili, Dr. Patrick Reardon, and Professor Moshe Gottlieb for insightful discussions regarding the collection and presentation of this data. This work was funded by the DOE Office of Science ASCR Program in Applied Mathematical Sciences and was supported by Los Alamos National Laboratory under U.S. Department of Energy Contract No. DE-AC52-06NA25396. Additional funding for this project was provided by the Los Alamos National Laboratory Directed Research and Development Program.

[1] J. R. Smart and D. T. Leighton, Phys. Fluids A **1**, 52 (1989).
[2] M. S. Ingber, A. A. Mammoli, P. Vorobieff, T. McCollam, and A. L. Graham, J. Rheol. **50**, 99 (2006).
[3] G. Barnocky and R. H. Davis, Phys. Fluids **31**, 1324 (1988).
[4] R. H. Davis, D. A. Rager, and B. T. Good, J. Fluid Mech. **468**, 107 (2002).
[5] A. N. Prokunin, Fluid Dyn. **38**, 443 (2003).
[6] J. Ashmore, C. del Pino, and T. Mullin, Phys. Rev. Lett. **94**, 124501 (2005).
[7] S. R. Challa and F. van Swol, Phys. Rev. E **73**, 016306 (2006).
[8] S. M. Tabatabaei, T. G. M. van de Ven, and A. D. Reya, J. Colloid Interface Sci. **301**, 291 (2006).
[9] M. A. Bevan and D. C. Prieve, Langmuir **15**, 7925 (1999).
[10] R. Cox and H. Brenner, Chem. Eng. Sci. **22**, 1753 (1967).
[11] R. H. Davis, J. Serayssol, and E. J. Hinch, J. Fluid Mech. **163**, 479 (1986).
[12] A. A. Kantak and R. H. Davis, Powder Technol. **168**, 42 (2006).
[13] H. Brenner, Chem. Eng. Sci. **16**, 242 (1961).
[14] A. D. Maude, Br. J. Appl. Phys. **16**, 242 (1961).
[15] J. Happel and H. Brenner, *Low Reynolds Number Hydrodynamics with Special Applications to Particulate Media* (Martinus Nijhoff, The Hague, Netherlands, 1983).
[16] R. B. Bird, W. E. Stewart, and E. N. Lightfoot, *Transport Phenomena* (Wiley, New York, 1960).
[17] A. J. Goldman, R. G. Cox, and H. Brenner, Chem. Eng. Sci. **22**, 637 (1967).
[18] R. I. Tanner, J. Fluid Mech. **17**, 161 (1963).
[19] A. L. Graham, L. A. Mondy, J. D. Miller, N. J. Wagner, and W. A. Cook, J. Rheol. **33**, 1107 (1989).
[20] V. Ilic, D. Tullock, N. Phan-Thien, and A. L. Graham, Int. J. Multiphase Flow **18**, 1061 (1992).
[21] C. E. Heath, M.S. thesis, University of New Mexico, 2007.
[22] R. G. Cox and H. Brenner, Chem. Eng. Sci. **22**, 1753 (1967).
[23] A. Vogel, W. Lauterborn, and R. Timm, J. Fluid Mech. **206**, 299 (1989).
[24] J. Franc and J. Michel, *Fundamentals of Cavitation* (Kluwer Academic, Dordrecht, Netherlands, 2004).
[25] W. J. Milliken, M. Gottlieb, A. L. Graham, L. A. Mondy, and R. L. Powell, J. Fluid Mech. **202**, 217 (1989).
[26] *Wyko Surface Profiler Technical Reference Manual* (Veeco Metrology Group, Tucson, USA, 1999).
[27] O. I. Vinogradova and G. E. Yakubov, Phys. Rev. E **73**, 045302(R) (2006).
[28] L. A. Mondy, A. L. Graham, P. Stroeve, and A. Majumdar, AIChE J. **33**, 862 (1987).
[29] P. T. Reardon, A. L. Graham, S. Feng, V. Chawla, R. S. Admuthe, and L. A. Mondy, Rheol. Acta **46**, 413 (2006).